Device-free RF human body fall detection and localization in industrial workplaces

Sanaz Kianoush, Stefano Savazzi, Federico Vicentini, Vittorio Rampa, and Matteo Giussani

***Abstract*—Fall detection and localization of human operators inside a workspace are major issues in ensuring a safe working environment. Recent research has shown that the perturbations of the radio-frequency (RF) signals commonly adopted for wireless communications can also be used as sensing tools for device-free human motion detection. Device-free RF-based human sensing applications range from tag-less body localization to detection and monitoring of human well-being (e-Health). In this paper, we propose a real-time system for human body motion sensing with special focus on joint body localization and fall detection. The proposed system continuously monitors and processes the RF signals emitted by industry-compliant radio devices operating in the 2.4 GHz ISM band and supporting machine-to-machine (M2M) communication functions. Human-induced diffraction and multipath phenomena that affect RF signal propagation are leveraged for body localization while for fall detection a Hidden Markov Model is applied to discern different postures of the operator and to detect safety-relevant events by tracking the received signal strength indicator footprints. Fall detection performances are corroborated by extensive experimental measurements in different settings. In addition, we propose also a sensor fusion tool that is able to integrate the device-free RF-based sensing system within an industrial image sensors framework. Preliminary results, conducted during field trial measurements, confirm the effectiveness of the proposed approach in terms of localization accuracy, and sensitivity/specificity to correctly detect a fall event from pre-impact postures.**

I. Introduction

Operator sensing is the topmost key issue in industrial workspace environments: it requires the extraction of information from operators in potentially harsh environments to model and understand their behavior from sensory data (*e.g.,* video, motion capture, audio). Detection of human behavior leverages common spatio-temporal information, namely location and activity. Industrial systems and solutions developed to detect and localize human motion can be based on wearable devices and sensors, such as accelerometers, wireless and posture sensors, camera/video data, or acoustic sources for event sensing [1].

S. Kianoush, S. Savazzi, and V. Rampa are with the Institute of Electronics, Computer and Telecommunication Engineering (IEIIT) of the National Research Council of Italy (CNR), Via G. Ponzio, 34/5, 20133 Milano, Italy, e-mail: {sanaz.kianoush, stefano.savazzi, vittorio.rampa}@ieiit.cnr.it.

F. Vicentini and M. Giussani are with the Institute of Industrial Technology and Automation (ITIA) of the National Research Council of Italy (CNR), Via E. Bassini, 15, 20133 Milano, Italy, e-mail: {federico.vicentini, matteo.giussani}@itia.cnr.it. M. Giussani is also with University of Brescia, Department of Information Engineering, via Branze 37, Brescia, Italy.

This work has been supported by the framework agreement Consiglio Nazionale delle Ricerche-Regione Lombardia, FIDEAS and CyberSort Projects.

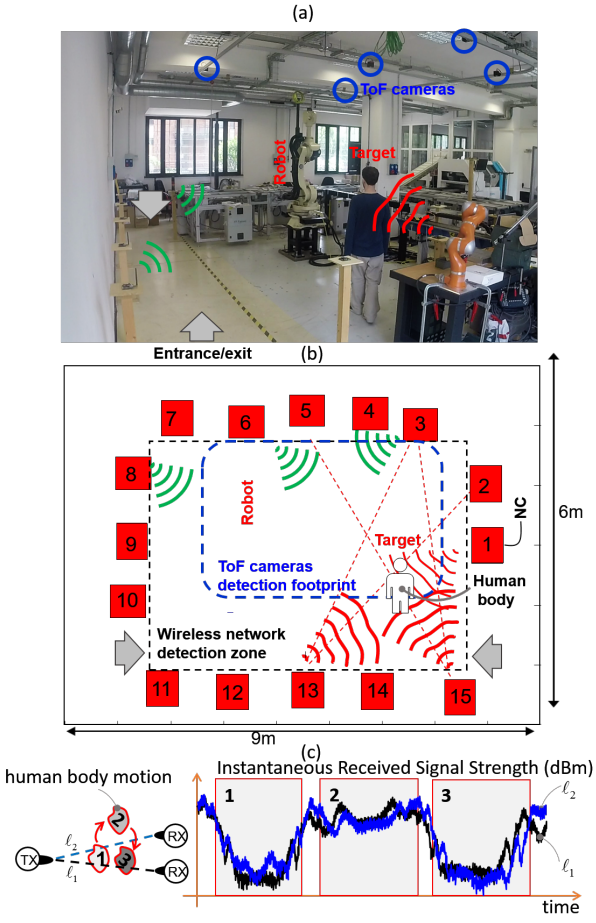

Fig. 1. (a) Picture of shared human-robot test environment with ToF cameras (*i.e.,* blue circles) and RF nodes, (b) deployment of the wireless network composed by RF nodes (*i.e.,* large red squares) and the corresponding detection zones for wireless network and ToF cameras that cover the monitoring positions, and (c) example of RF signal inspection for human sensing inside the detection area of a dual-link scenario.

Body-worn sensing devices may have a substantial footprint on users (*i.e.,* tracked subjects) and might hinder their working activities. Systems based on cameras, video or acoustic sources are also effective but are typically penalized by limited ranges, major occlusions problems, and privacy concerns. On the other hand, proliferation of wireless connected radio devices as part of the Internet of Things (IoT) paradigm is acting as a boost to the development of new radio-frequency (RF) based recognition technologies [2]. Recent research shows that the perturbations of the RF fields usually adopted for wireless transmissions (*i.e.,* in the 2-5 GHz ISM bands) can be also

used as a powerful sensing tool for several ambient intelligence services, ranging from plain detection of human body motion to precise localization [3] [4]. Radio devices deployed in an industrial space can therefore not only serve as interfaces for ubiquitous machine-to-machine (M2M) communication, but they are also expected to incorporate novel or augmented sensing capabilities with the goal of acquiring an accurate human-scale understanding of space and motion.

In this paper, we propose a novel RF-based device-free approach for fall detection and operator localization. The proposed system is designed to continuously monitor the fluctuations of the RF field measured, across a workspace, by a dense network of radio devices (see Fig. 1). These devices, that are part of a pre-existing or a newly deployed network, are placed at arbitrary locations around the monitored area. The presence, position, and motion of the human body affect both the RF signal attenuation and the multipath propagation in a predictable way. It makes possible to estimate and track human location and activity without the need to deploy and calibrate additional wearable sensors (device-free detection), neither to ask for specific user actions (non-cooperative detection). Sensing of human body is thus based on the continuous monitoring of the radio channel quality, namely the Received Signal Strength Indicator (RSSI). Human activities, defined as the set of non-rigid body motions, leave a characteristic footprint on the RSSI observed patterns. Focusing on body falling, *i.e.,* from standing/walking to ground posture, RF fluctuations increase during the earliest stage of fall, *i.e.,* in the descent phase (pre-impact), while they reduce to stable configuration corresponding to the body lying on the floor.

The aim of this paper is to promote the integration of RF-based device-free human sensing technology into an industry-compliant architecture by verifying its ability to jointly support both human localization and fall detection (in the surroundings of the body location) and in turn to provide augmented information about worker safety. Existing solutions to the fall detection problem [5] [6] can gain only partial confidence by users about their reliability for the deployment in real industrial environments. Provided that no single technology can solve the problem of continuous worker monitoring (*e.g.,* fall detection, localization, status of proximity to machines, onset of hazardous events), a solid evidence in detection performance is the major driver for system design choices. According to this vision, the proposed solution is designed to be integrated into a worker-sensing ecosystem, *i.e.,* a combination of multiple sensor sources and technologies: it makes use of an existing distributed wireless network infrastructure deployed for standard M2M communication tasks and enables an augmented virtual sensing service on top of it. Industry-standard wireless devices (*e.g.,* WiFi, IEEE 802.15.4) are adopted for performance assessment. System validation is based on both IEEE 802.15.4 standard-compliant nodes and Software Defined Radio (SDR) devices emulating the physical (PHY) layer of the WiFi IEEE 802.11g standard. Finally, the design and the experimental validation of a sensor fusion framework is also addressed to integrate the device-free RF-based human sensing technology with image sensors (*i.e.,* 3D Time-of-Flight cameras).

II. Related work and contributions

One of the most important applications for Internet of Things is human sensing in smart spaces (*e.g.,* workplaces and homes), where human activities generate lots of data from the interaction with IoT-based environments [7]. These rich interaction data can be further processed and modeled as useful contexts to provide appropriate services accordingly. Systems and solutions developed for human sensing can be divided into two main families according to the sensing technologies employed. The first approach is based on the use of wearable devices and sensors, such as accelerometers, wireless and posture sensors [8] [9]. The second one, classified as context-aware, is based on camera/video devices, acoustic sources and/or other event sensors [1]. While most of the research on human sensing have focused on device-based technologies (*e.g.,* smart phone sensors such as accelerometers, magnetometers, gyroscopes, GPS devices, microphones, and cameras) [5] [10] [11], looking to the industrial domain, the trend towards these solutions poses several problems [12] [13]. For example, personal protective equipment in the workplace involves wearable devices that are designed to protect only the single individual, while in the context of functional safety, not all plant operators are supposed to wear a personal radio tag. Wearable devices also strongly limit operator mobility, visibility, and communication during working tasks.

Alternatively, device-free recognition systems may exploit the properties of *reflectivity* with time-of-flight cameras or radars, *attenuation* with tomographic sensors, or *emissivity* with thermal images to extract human position and gestures [14] [15]. While the main advantage of using device-free approaches is that the operator does not need to wear any device, they usually focus on acoustic/audio sensors [16] [17] or vision-based solutions [18]. However, these approaches are typically characterized by high installation costs, limited detection range, long calibration setup time as well as privacy constraints. Finally, they cannot be used in case of fire or in presence of smoke.

The use of embedded RF nodes for device-free human sensing, as proposed in this paper, provides a number of advantages in industrial workspaces: with respect to other sensing systems, the RF devices rely in fact on inexpensive commercial radio nodes operating in the unlicensed bands (*e.g.,* 2.4 GHz and 5.8 GHz ISM bands). In addition, the technology allows to track human body movements by analyzing the perturbations of the same RF field adopted for wireless data communication, and thus by leveraging the existing networking infrastructure as a powerful software-defined sensing tool. Unlike optical and infrared technologies, RF waves are insensitive to visual obstruction (*e.g.,* due to the presence of smoke or occluding materials) and can also penetrate nonmetallic walls. Compared to wired security and surveillance systems, the RF-based approach reduces both cost and installation time, and it is flexible enough to be easily installed in different areas of interest, if required. On the other hand, the low cost of each unit leads to deploy several nodes that are able to cover larger areas, thus increasing systems scalability.

A few device-free RF-based systems are known in the liter-

ature [19] [20] [21]. The work in [21], for instance, proposes a Device-Free Localization (DF-L) system that makes use of stochastic modeling of RSSI data as a function of the target location. In [19] statistical anomaly detection techniques and particle filtering are applied while the system adapts to small changes in rich multipath environments. The tomographic method in [20] allows to visually inspect and provide an accurate radio imaging of the area of interest.

The novel contributions introduced by this work are related to: i) definition of algorithms for joint localization and fall detection of operators inside the industrial area; ii) real-time system implementation of the proposed algorithms, and iii) validation of the proposed system implementation through an extensive field measurement campaign.

Compared to previous works in this field, the proposed device-free RF system processes the wireless channel quality information for the $joint$ human localization and detection of body falling. Physical-layer channel quality information can be collected and processed before decoding (base-band) or after decoding (*i.e.,* in the upper layers): in both cases this is measured in terms of RSSI.

Two case studies are considered. In the first one, base-band extraction and processing of RSSI data are carried out through SDR devices that emulate the physical layer of a WiFi-compliant IEEE 802.11g link (see also [19] for related research). In the second case, RSSI samples are extracted from consecutive physical layer IEEE 802.15.4-compliant data frames. Operator localization is based on Bayesian techniques [21]. Instead, motion (fall) recognition is based on the real-time analysis of RSSI sequences (or footprints), modeled by a Hidden Markov Model (HMM).

Extensive experimental analysis confirms that both transition states and observation probabilities characterizing the HMM parameters can be automatically trained and provide a reliable indicator for real-time motion detection, also effectively counter-balancing human-induced time-warping effects on sequences due to arbitrary body motions.

The RF system is integrated into an industry-relevant worker sensing ecosystem supporting 3D image sensors: a sensor-fusion approach is implemented to effectively combine the benefits of both information sources (*i.e.,* from RF devices and 3D Time-of-Flight cameras) for the purpose of fast real-time estimation of the operator motion.

The paper is organized as follows: methods for device-free localization are summarized in Sect. III, while validation of the sensor fusion framework for body sensing is illustrated in Sect. IV, focusing on the problem of operator detection inside a human-robot shared workspace area [21]. Sect. V introduces a general HMM-based method for joint DF-L and activity recognition while Sect. VI describes an experimental case study on Device Free Fall Detection (DF-FD) as a particular case of activity recognition processing. Conclusions are drawn in Sect. VII.

III. Device-free human body localization (DF-L)

Device-free human localization and tracking is carried out by processing, in real-time, RSSI measurements taken over multiple links by wireless devices deployed in the monitoring area. Note that the operator does not need to carry any electronic device and he/she is assumed to freely move within the detection area by covering the locations $\mathbf{x}_t \in \{\mathbf{H}_m\}_{m=0}^{N_H} = \bar{\mathcal{H}}$, with $\mathbf{x}_t = \mathbf{H}_0$ indicating the operator located outside the detection zone and N_H the number of monitored positions $\mathbf{H}_m$. Detection of human activities assumes that the position $\mathbf{x}_t$ of the operator in the workspace at time t is known or estimated ($\widehat{\mathbf{x}}_t$) according to the methods summarized in this section.

The system under consideration consists of a (pre-existing or ad-hoc placed) deployment of N wireless devices placed at arbitrary locations that perform synchronous RSSI measurements from L peer-to-peer links, forwarding them to a Gateway node serving as network coordinator (NC) (see the simplified setting in Fig. 1) and processing unit.

A single target (*e.g.,* an operator) is assumed to move within the detection area for the purpose of being (anonymously) tracked. During such movements, at discrete time instants $t = 1, 2, 3, \ldots$, the processing unit NC collects the set of L noisy power measurements $\mathbf{s}_t = [s_{1,t} \cdots s_{L,t}]^T$, where each observation $s_{\ell,t}$ represents RSSI values measured on the link $\ell \in \mathcal{L} = \{1, \ldots, L\}$, at the t-th time instant. The target position $\mathbf{x}_t$ is not directly observable since its induced RF perturbations are embedded into the noisy RSSI measurements $\mathbf{s}_t$.

Stochastic modeling can be adopted to relate the RSSI measurements over each link to the target position. Since the presence of the target affects both the attenuation and the random fluctuations of the received power, a log-normal model is defined where the RSSI mean and variance are expressed as functions of the target location. The increase of path-loss and power fluctuation induced by the moving target can be described by exploiting the theory of diffraction [22]. In case of target movements, the measured RSSI value $s_{\ell,t}(\mathbf{x}_t)$ is affected by an additional perturbation that depends on the specific position $\mathbf{H}_m$ and is characterized, $\forall \ell \in \mathcal{L}$, in terms of absence (*i.e.,* $\mathbf{x}_t = \mathbf{H}_0$) or presence (*i.e.,* $\mathbf{x}_t = \mathbf{H}_m$) of the target in the covered area as

$$s_{\ell,t}(\mathbf{x}_t) = \begin{cases} \mu_\ell(\mathbf{H}_0) + w_\ell(\mathbf{H}_0), & \text{if } \mathbf{x}_t = \mathbf{H}_0 \\ \mu_\ell(\mathbf{H}_m) + w_\ell(\mathbf{H}_m), & \text{if } \mathbf{x}_t = \mathbf{H}_m. \end{cases} \quad (1)$$

Both deterministic path-loss $\mu_\ell(\mathbf{H}_m)$ and random fading $w_\ell(\mathbf{H}_m) \propto N(0, \sigma_\ell^2(\mathbf{H}_m))$ embed the information about the object position $\mathbf{H}_m$

$$\mu_\ell(\mathbf{H}_m) = \mu_\ell(\mathbf{H}_0) - \Delta\mu_\ell(\mathbf{H}_m) \quad (2)$$

where $\Delta\mu_\ell(\mathbf{H}_m)$ is the additional variation of attenuation due to the obstruction of the links caused by the human presence. An increased RSSI variability is also observed as

$$\sigma_\ell(\mathbf{H}_m) = \sigma_\ell(\mathbf{H}_0) + \Delta\sigma_\ell(\mathbf{H}_m) \quad (3)$$

where $\Delta\sigma_\ell(\mathbf{H}_m)) \geq 0$ denotes the corresponding increased standard deviation. For position estimation, the knowledge of the reference parameters from RSSI $\{\mu_\ell(\mathbf{H}_0), \sigma_\ell(\mathbf{H}_0)\}$, for

the operator outside the monitoring area, is required for all links $\ell \in \mathcal{L} = \{1, \ldots, L\}$, together with the information about the perturbation maps $\{\Delta\mu_\ell(\mathbf{x}_t), \Delta\sigma_\ell(\mathbf{x}_t)\}$ for all position values $\mathbf{x}_t = \mathbf{H}_m$. While $\{\mu_\ell(\mathbf{H}_0), \sigma_\ell(\mathbf{H}_0)\}$ can be easily pre-calibrated when no target is moving in the network area, evaluation of profiles $\{\Delta\mu_\ell(\mathbf{H}_m), \Delta\sigma_\ell(\mathbf{H}_m)\}$ requires extensive fingerprinting campaigns [20] or ray-tracing simulations [23]. Once the maps $\{\Delta\mu_\ell(\mathbf{H}_m), \Delta\sigma_\ell(\mathbf{H}_m)\}$ have been built, the target location $\widehat{\mathbf{x}}_t = \mathbf{H}_m$ can be estimated. In what follows, different DF-L methods are investigated.

A. Maximum likelihood method (ML)

Target localization can be based on the maximum likelihood estimation (ML) algorithm [4]. The joint log-likelihood function $\Lambda(\mathbf{s}_t|\mathbf{H}_m)$ is evaluated, $\forall m = 0, ..., N_H$ as

$$\Lambda(\mathbf{s}_t|\mathbf{H}_m) = \sum_{\ell=1}^{L} \ln\left[P(s_{\ell,t}|\mathbf{H}_m)\right] \tag{4}$$

where, for the RSSI sample $s_{\ell,t}$, it is

$$P(s_{\ell,t}|\mathbf{H}_m) = \frac{1}{(2\pi)^{1/2}\sigma_\ell(\mathbf{H}_m)} \exp\left\{-\frac{1}{2}\frac{\left[s_{\ell,t} - \mu_\ell(\mathbf{H}_m)\right]^2}{\sigma_\ell^2(\mathbf{H}_m)}\right\}.$$

Target location is obtained as $\widehat{\mathbf{x}}_t = \mathbf{H}_m$ where

$$\widehat{\mathbf{x}}_t = \underset{\mathbf{H}_m \in \bar{\mathcal{H}}}{\operatorname{argmax}} \quad \Lambda(\mathbf{s}_t|\mathbf{H}_m). \tag{5}$$

B. Bayesian methods

The Bayesian approach for DF-L [19], [21] iteratively updates the *a-posterior* probability $\Gamma_x(\mathbf{H}_m) = P(\mathbf{x}_t = \mathbf{H}_m \mid \mathbf{S}_t)$ for all positions $\mathbf{x}_t = \mathbf{H}_m$ with $\mathbf{S}_t = [\mathbf{s}_1, ..., \mathbf{s}_t]^T$ collecting all RSSI measurements taken over the $\ell \in \mathcal{L}$ links up to time t. A-posterior probability $\Gamma_x(\mathbf{H}_m)$ at time t is obtained as

$$\Gamma_x(\mathbf{x}_t = \mathbf{H}_m) \propto P(\mathbf{s}_t \mid \mathbf{H}_m) \times P(\mathbf{x}_t = \mathbf{H}_m \mid \mathbf{S}_{t-1}) \tag{6}$$

where $P(\mathbf{s}_t \mid \mathbf{H}_m)$ is the joint likelihood and depends on human-induced RSSI perturbations (2) and (3) while *a priori* probability $P(\mathbf{x}_t = \mathbf{H}_m \mid \mathbf{S}_{t-1})$ is iteratively updated as

$$\begin{gathered} P(\mathbf{x}_t = \mathbf{H}_m \mid \mathbf{S}_{t-1}) = \\ = \textstyle\sum_{n=0}^{N_H} P(\mathbf{x}_t = \mathbf{H}_m \mid \mathbf{H}_n) \times P(\mathbf{x}_{t-1} = \mathbf{H}_n \mid \mathbf{S}_{t-1}) \end{gathered} \tag{7}$$

where N_H is the number of monitored positions. The state transition probability $P(\mathbf{x}_t = \mathbf{H}_m \mid \mathbf{x}_{t-1} = \mathbf{H}_n)$ is function of the target motion model. The movements of the operator are modeled by the 2D Gaussian random walk

$$\mathbf{x}_t = \mathbf{x}_{t-1} + \mathbf{v}_t \tag{8}$$

with Circular Gaussian random driving process $\mathbf{v}_t$ with deviation corresponding to the maximum human body speed (typically 3 samples for 1 m/s).

For positioning, the maximum *a-posteriori* (MAP) estimation can be adopted

$$\widehat{\mathbf{x}}_t = \underset{\mathbf{H}_m \in \bar{\mathcal{H}}}{\operatorname{argmax}} \quad \Gamma_x(\mathbf{H}_m). \tag{9}$$

Alternatively, minimum mean square error (MMSE) estimator can be obtained as

$$\widehat{\mathbf{x}}_t = \mathbb{E}[\mathbf{x}_t = \mathbf{H}_m \mid \mathbf{S}_t] = \sum_{\mathbf{H}_m \in \bar{\mathcal{H}}} \mathbf{H}_m \times \Gamma_x(\mathbf{H}_m). \tag{10}$$

The pseudo-code for Bayesian DF-L method is shown in the Algorithm 1 diagram below, including two main procedures: calibration and real time localization.

Most of DF-L Bayesian methods are limited to slowly changing scenarios; however the use of an ad-hoc interactive multiple model (IMM) approach has been shown in [21] to effectively capture the RF perturbations induced by the changing environment (*e.g.,* caused by concurrently moving robots), and thus isolate the RSSI perturbations induced by the human body.

Algorithm 1 DF-L

procedure CALIBRATION
  for $\ell = 1 : L$ **do**
    $\{\Delta\mu_\ell(\mathbf{H}_m), \Delta\sigma_\ell(\mathbf{H}_m)\}$ ← `build up the RSS map from the reference measurements` $\bar{\mathbf{S}}_\ell$
    $P(\mathbf{x}_0 \mid \mathbf{S}_0) \leftarrow$ `initialize at t=0`
  end for
end procedure
procedure REAL TIME LOCALIZATION ($t > 0$)
  for $m = 0 : N_H$ **do**
    $P(\mathbf{s}_t \mid \mathbf{H}_m) \leftarrow$ `joint likelihood (4)`
    $P(\mathbf{x}_t = \mathbf{H}_m \mid \mathbf{S}_t) = P(\mathbf{s}_t \mid \mathbf{H}_m) \times P(\mathbf{x}_t = \mathbf{H}_m \mid \mathbf{S}_{t-1}) \leftarrow$ `a-posterior probability (6)`
    $P(\mathbf{x}_t = \mathbf{H}_m \mid \mathbf{S}_{t-1}) \leftarrow$ `update (7)`
  end for
  $\widehat{\mathbf{x}}_t = \underset{\mathbf{H}_m \in \bar{\mathcal{H}}}{\operatorname{argmax}} \; P(\mathbf{x}_t = \mathbf{H}_m \mid \mathbf{S}_t) \leftarrow$ `location estimation(9)`
end procedure

IV. DF-L: SYSTEM VALIDATION IN INDUSTRIAL WORKPLACES

The DF-L service that adopts the Bayesian algorithm with MAP estimation and profile $\{\Delta\mu_\ell(\mathbf{H}_m), \Delta\sigma_\ell(\mathbf{H}_m)\}$ evaluation by fingerprinting measurements, is validated in realistic conditions inside a controlled testing pilot plant (see Fig. 1 (a)). The configuration adopted for the test plant is similar to a typical robotic-assisted industrial scenario where a single operator interacts with a robot (*e.g.,* a robotic manipulator for handling/assembling tasks) placed in a fixed position inside a fenceless area (*i.e.,* a workplace unit). The collaborative shared workspace, covered by the DF-L system, is also monitored by a set of 5 Time-of-Flight (ToF) ceiling-mounted cameras [24] that provide 3D depth mapping of the target region. Boundary regions of each camera are overlapped among two or more sensors, in order to limit the degradation of the detection accuracy with the distance from the center of their Field-of-View (FoV). The whole set of cameras provides a single merged information about the position of a moving target (*e.g.,* operator). The target is detected in the form of an enveloped

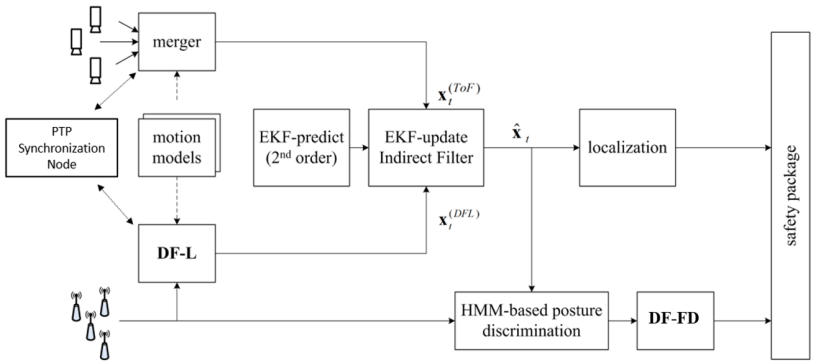

Fig. 2. Integrated sensor fusion scheme for localization and fall detection modules, all concurring as multiple inputs to a safety package for worker protection.

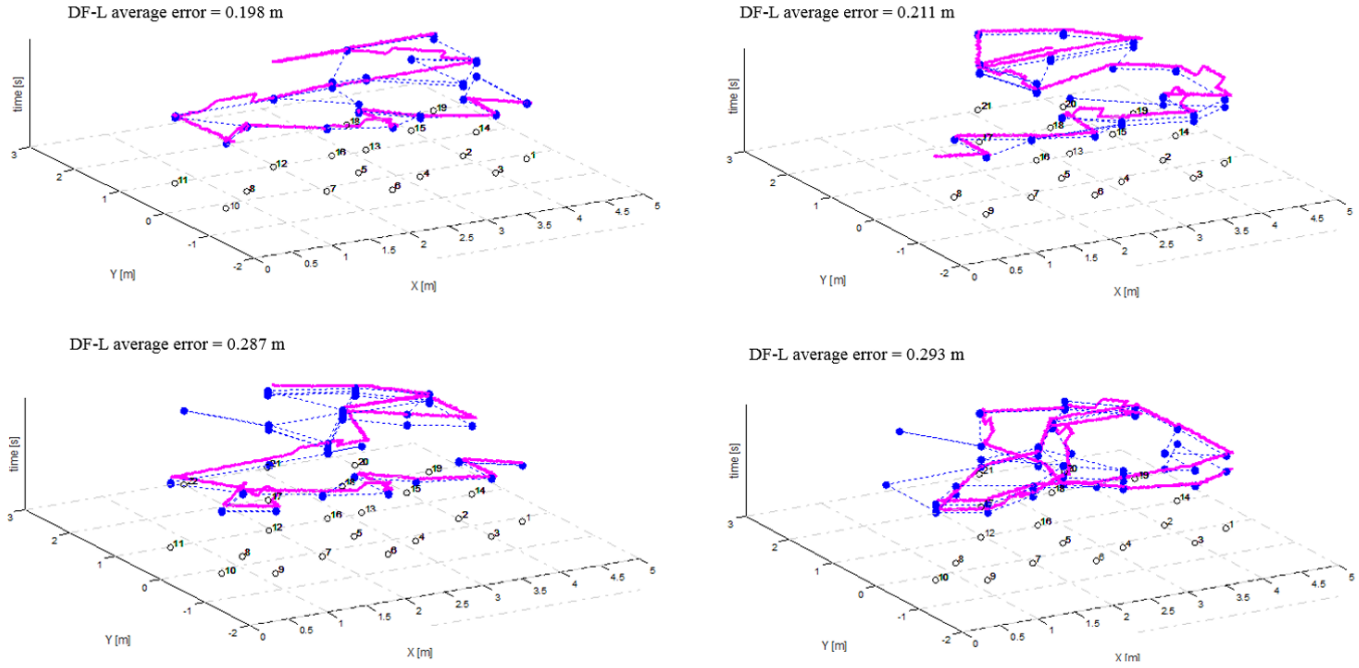

Fig. 3. Four different human trajectories inside the plant, tracked from ToF (magenta) and DF-L (blue) with corresponding average error.

cloud of clustered pixels, whose centroid coordinates are filtered and extracted.

The ToF set is mainly used in a validation experiment that includes 4 trajectories, simultaneously obtained by the DF-L service under validation. In order to have an absolute time reference, data from both sources are recorded by an additional node and synchronized using the IEEE 1588 Precision Time Protocol (PTP) [25].

Each trajectory is obtained from an average-size human target (1.70 m tall, 65 kg), walking along different paths, *i.e.,* passing approximately over the calibrated locations and maintaining an almost constant speed in the range of $0.5-0.8$ m/s. Recorded patterns are reported in Fig. 3. While the ToF cameras provide the validation trace (*golden standard*), the DF-L channel extracts the estimated positions corresponding to the calibrated locations. The estimated DF-L path is therefore represented in form of discrete jumps into reference locations, *i.e.,* places where the a-posteriori probability of occupancy is largest at each time step.

The accuracy metric for validation is the average error of DF-L localization w.r.t. the reference ToF pattern (this is also superimposed in Fig. 3 for each trajectory). DF-L localization errors appear in form of sudden jumps to non-occupied locations. Most of errors occur in proximity of the robot body (see the position of the robot in Fig. 1). Recall that the robot is not moving, but still represents a massive disturbance contribution in direct and nearby RF links.

DF-L accuracy for the considered trajectories, expressed in root mean squared error (RMSE) is below 0.3 m, while the sample rate of the output estimates is equal to 360 ms. DF-L accuracy typically depends on the number of available links and the grid size adopted for the reference locations.

The fundamental limits to the DF-L positioning accuracy can be also evaluated for a generic configuration of networked nodes [26]. Even if the observed accuracy and sample rates are larger for ToF, the availability of alternative sources of localization is beneficial for the human tracking capability inside the workspace.

As shown in ToF signals (see Fig. 3), range sensors may momentarily be subject to error conditions, which are chiefly due to possibly changing environmental lighting conditions, degree of the object's reflective properties, color, gloss and complexity of the scene. Background light, whether artificial or sunlight and interference by several ToF cameras running at the same time may also cause errors in the working environment. Adaptive filters, in fact, might not be able to react to such sudden changes. Additionally, the boundary FoV is less accurate and potentially affected by misplaced pixels.

Such disadvantages of the image range sensors, together with the high cost of the technology, may in fact be mitigated by the concurrent use of RF technology. Specifically due to the cost limitations, ToF sensors tend to be limited in number so as to reduce the covered workspace. Widely available wireless nodes and simple implementation in industrial layouts are supporting factors for integrating the DF-L system into the human tracking service.

For the purpose of safely using both image ToF cameras and the wireless DF-L nodes, a software tool for sensor fusion has been implemented on top of the ToF framework. In such scheme, the ToF channel is considered as one of the sources to be fused, yet the fastest and the most accurate [24]. Input data from the ToF and the DF-L channels are sampled at 60 ms. However, the output from the DF-L system is computed every 6 samples. The fused results are available every 60 ms [21].

As a matter of design, the runtime location of the target obtained from the DF-L as $\hat{\mathbf{x}}_t = \mathbf{x}_t^{DFL}$ (see Fig. 2) is fused with the tracking location $\hat{\mathbf{x}}_t = \mathbf{x}_t^{ToF}$ from the ToF cameras. The fusion of sensor sources is done inside the update step of a standard Extended Kalman Filtering (EKF) as in [27]. The update step is in the form of Indirect Filter [28], which plainly merges the fusing sources without pre-filtering and/or feedforwarding/feedbacking. The EKF prediction (a-priori estimation) is implemented as a model-based estimation of human walking based on second-order kinematics [29]. Both sources (*i.e.,* DF-L and ToF cameras) have a sample rate slower than desired *e.g.,* synchronization with robot control rate ($500 - 1000$ Hz). The EKF prediction stage is therefore oversampled w.r.t. the update stage in order to provide a timely, even if less accurate, estimation of location in absence of actual data. The inaccuracy of fused information is derived from the EKF covariance.

The resulting estimation of the target location $\widehat{\mathbf{x}}_t$ may be directly used for the purpose of human tracking (*e.g.,* obstacle avoidance in the case of human-robot shared workspace) and for injecting positional information in the DF-FD function (Fig. 2).

V. Location-aware device-free activity recognition

Analysis of human-induced RSSI fluctuations in a given position as described in (2) and (3) is carried out in this section to identify generic, or possibly safety-relevant full-body gestures or activities (*i.e.,* a body fall) in the surroundings of the operator location. The system is herein designed to identify and discriminate N_F human body actions $\mathcal{F} := \{F_n\}_{n=0}^{N_F}$ modeled as consecutive non-rigid body motions of a person located in a given position $\mathbf{x}_t \in \bar{\mathcal{H}}$ inside the monitoring area. F_0 represents any safe activity of no interest for recognition purposes (*i.e.,* a human $safe$ state). Activity F_n ($n > 0$) results in a pattern of RSSI sequences $s_{\ell,t}(\mathbf{x}_t)$ with predictable stochastic properties: activity detection is carried out by assuming that the operator is located at known position $\mathbf{x}_t$. Location can be also estimated as $\hat{\mathbf{x}}_t = \mathbf{H}_m$ using the previous DF-L methods shown in Sect. III. Activity detection is based on real-time processing of human-induced RSSI sequences measured during consecutive radio transmissions. The fall detection activity is specifically addressed in Sect. V-B.

To increase the detection accuracy and limit the real-time computational processing requirements, the RSSI measurements are restricted only to a subset of links $\mathcal{L}_{\mathbf{x}_t=\mathbf{H}_m} = \mathcal{L}_{\mathbf{H}_m} \subset \mathcal{L}$. This subset is selected during the initial off-line training step to reduce the computational requirements as described in Sect. V-B. Using the same approach already shown in Sect. III, we define the sequence of T consecutive RSSI observations corresponding to a human activity F_n in position $\mathbf{H}_m$ as $\mathbf{S}_\ell = \mathbf{S}_\ell(F_n|\mathbf{H}_m) = [s_{\ell,1}, s_{\ell,2}....s_{\ell,T}]$, with $s_{\ell,t}$ being the RSSI observed at time $1 \leq t \leq T$ and over a wireless link $\ell \in \mathcal{L}_{\mathbf{H}_m}$: in particular

$$s_{\ell,t}(F_n|\mathbf{H}_m) = \mu_\ell(\mathbf{H}_m) + \triangle s_{\ell,t}(F_n|\mathbf{H}_m). \qquad (11)$$

The RSSI footprint $\triangle\mathbf{S}_\ell(F_n|\mathbf{H}_m) = [\triangle s_{\ell,1}, \triangle s_{\ell,2}.... \triangle s_{\ell,T}]$ collects the RSSI deviations (or shifts) observed over link ℓ and with respect to the average RSSI observed for human located in corresponding position $\mathbf{H}_m$, while $\mu_\ell(\mathbf{H}_m)$ is defined as in (2). Since the human state is not directly observable and is hidden in the corresponding RSSI shifts, an Hidden Markov Model-based (HMM) approach is adopted for detection. Hidden states are chosen to model the $embedded$ temporal sequence of the RSSI shifts $\triangle s_{\ell,t}(F_n|\mathbf{H}_m)$. States transition probabilities are designed to account for possible time-warping effects during real-time activity recognition. In the following section, we investigate the fundamental problems regarding HMM design for device-free activity recognition, namely: the specification of HMM model parameters, the model adjustments to best account for the noisy observed signals and the HMM evaluation phase.

A. Hidden Markov Model-based activity recognition

In this section, the RSSI shifts $\triangle s_{\ell,t}(F_n|\mathbf{H}_m)$ are described by a HMM model whose parameters depend on the monitored link ℓ, the human activity F_n and the estimated position $\mathbf{H}_m$. The HMM states $\mathbf{Q}_\ell(F_n|\mathbf{H}_m) = [\mathrm{q}_j]_{j=1}^{N_\ell}$ contain N_ℓ selected values q_j from the footprints $\triangle\mathbf{S}_\ell(F_n|\mathbf{H}_m)$

learned during the training stage. The HMM parameters $\lambda_\ell(F_n|\mathbf{H}_m) := [\mathbf{A}_\ell, \mathbf{B}_\ell, \boldsymbol{\pi}_\ell]$ are the human motion transition state $[\mathbf{A}_\ell]_{i,j} = P[q_{t+1} = \mathrm{q}_i | q_t = \mathrm{q}_j]$, the observation probability $[\mathbf{B}_\ell]_{k,j} = P[s_{\ell,t} = \mathrm{s}_k | q_t = \mathrm{q}_j]$ and the initial state probability $[\boldsymbol{\pi}_\ell]_i = P[q_0 = \mathrm{q}_i]$ (for $t = 0$). The HMM parameters are evaluated according to the Baum-Welch algorithm [30] and trained for each selected link $\ell \in \mathcal{L}_{\mathbf{H}_m}$.

The detection system iteratively computes the log-likelihood functions $\Lambda_\ell\left[\mathbf{S}_\ell|F_n, \mathbf{H}_m\right] = \ln P\left[\mathbf{S}_\ell|\lambda_\ell\right]$ of the observation sequence for each activity F_n and using the HMM parameters corresponding to the estimated body position $\hat{\mathbf{x}}_t = \mathbf{H}_m$. Each log-likelihood function $\Lambda_\ell\left[\mathbf{S}_\ell|F_n, \mathbf{H}_m\right]$ is obtained iteratively (*i.e.,* during the evaluation phase) as

$$\Lambda_\ell\left[\mathbf{S}_\ell|F_n, \mathbf{H}_m\right] = \ln\left(\sum_{\mathbf{q}\in\mathbf{Q}_\ell(F_n|\mathbf{H}_m)} P[\mathbf{S}_\ell, \mathbf{q}|\lambda_\ell]\right), \quad (12)$$

with state sequence $\mathbf{q} = [q_1, ..., q_T]^{\mathrm{T}}$ and joint probability $P[\mathbf{S}_\ell, \mathbf{q}|\lambda_\ell] = \prod_{t=1}^{T} P[s_{\ell,t}|q_t] \cdot P[q_t|q_{t-1}]$. Functions in (12) are continuously evaluated for new observed sequences over the selected links.

Decision on activity $\widehat{F}_n$ can be made by maximizing the sum of the log-likelihood terms

$$\Lambda(F_n, \mathbf{H}_m) = \sum_{\ell\in\mathcal{L}_{\mathbf{H}_m}} \Lambda_\ell\left[\mathbf{S}_\ell|\mathrm{F}_n, \mathbf{H}_m\right] \quad (13)$$

as

$$\widehat{F}_n = \underset{F_n\in\mathcal{F}}{\operatorname{argmax}} \quad \Lambda(F_n, \mathbf{H}_m). \quad (14)$$

B. Body fall detection (DF-FD) and system calibration

For system validation, the techniques illustrated in Sect. V-A are herein adopted to discriminate operator falling (described as state F_1 or *fall* state) from a safe condition (indicated as F_0 or *non-fall* state) corresponding to a human located in a known position $\mathbf{x}_t$ inside the detection zone and in safe conditions (*i.e.,* sitting, standing or walking inside the detection area). Fall detection is based on hard decisions over an optimized subset of links $\ell \in \mathcal{L}_{\mathbf{H}_m}$ selected during a calibration procedure, while non informative links are purged.

Calibration of DF-L and DF-FD systems is implemented by an automatic software tool collecting RSSI reference measurements: at first, it acquires and processes $\bar{\mathbf{S}}_\ell(\mathbf{H}_0)$ values when no target is inside the area, and then $\bar{\mathbf{S}}_\ell(F_1, \mathbf{H}_m)$ and $\bar{\mathbf{S}}_\ell(F_0, \mathbf{H}_m)$ for human body in safe and non-safe state for each position $\mathbf{H}_m$ of interest, respectively. Calibration of the DF-L model parameters requires the estimation of deviations $\Delta\mu_\ell(\mathbf{H}_m)$ and $\Delta\sigma_\ell(\mathbf{H}_m)$ as described in (2) and (3). During this process a person moves along a predefined training path that spans all covered positions $\mathbf{H}_m$ while the processing unit collects and synchronizes the RSSI measurements $\bar{\mathbf{S}}_\ell(F_0, \mathbf{H}_m)$ received from the wireless devices. These are used to evaluate the sample average $\mu_\ell(\mathbf{H}_m) = \mathbb{E}\left[\bar{\mathbf{S}}_\ell(F_0, \mathbf{H}_m)\right]$ and the sample standard deviation $\sigma_\ell(\mathbf{H}_m) = \mathrm{std}\left[\bar{\mathbf{S}}_\ell(F_0, \mathbf{H}_m)\right]$. From these measurements, it is then easy to compute the DF-L parametric maps $\Delta\mu_\ell(\mathbf{H}_m)$ and $\Delta\sigma_\ell(\mathbf{H}_m)$.

The calibration of the HMM parameters $\lambda_\ell(F_1|\mathbf{H}_m)$, $\lambda_\ell(F_0|\mathbf{H}_m)$ for fall detection is carried out by the expectation-maximization algorithm, also known as Baum-Welch algorithm, using the corresponding reference sequences $\bar{\mathbf{S}}_\ell(F_1, \mathbf{H}_m)$, $\bar{\mathbf{S}}_\ell(F_0, \mathbf{H}_m)$ for body falling in position $\mathbf{H}_m$. Selection of the link subset $\mathcal{L}_{\mathbf{H}_m}$ for each monitored position $\mathbf{H}_m$ is obtained as shown in the next paragraph.

Link selection. Optimization of the link subset $\mathcal{L}_{\mathbf{H}_m}$ is based on the log-likelihood terms (12): for each link, log-likelihood ratio metrics are evaluated from reference measurements, *i.e.,* fall ratio (FR) and non-fall ratio (NR) values. The log-likelihood metric evaluation for F_1 vs. F_0 compares fall $\Lambda_\ell\left[\bar{\mathbf{S}}_\ell|F_1, \mathbf{H}_m\right]$ vs. non-fall $\Lambda_\ell[\bar{\mathbf{S}}_\ell|F_0, \mathbf{H}_m]$ likelihood functions using as reference observations the input sequences corresponding to a human body falling

$$\mathrm{FR}_\ell(\bar{\mathbf{S}}_\ell) = \Lambda_\ell\left[\bar{\mathbf{S}}_\ell|F_1, \mathbf{H}_m\right] - \Lambda_\ell[\bar{\mathbf{S}}_\ell|F_0, \mathbf{H}_m], \quad (15)$$

with $\bar{\mathbf{S}}_\ell = \bar{\mathbf{S}}_\ell(F_1, \mathbf{H}_m)$. Similarly, the metric evaluation for F_0 vs. F_1 compares non-fall and fall probability using non-fall measurements as reference observations

$$\mathrm{NR}_\ell(\bar{\mathbf{S}}_\ell) = \Lambda_\ell[\bar{\mathbf{S}}_\ell|F_0, \mathbf{H}_m] - \Lambda_\ell[\bar{\mathbf{S}}_\ell|F_1, \mathbf{H}_m], \quad (16)$$

with $\bar{\mathbf{S}}_\ell = \bar{\mathbf{S}}_\ell(F_0, \mathbf{H}_m)$. Optimal link subset is thus obtained by selecting only the links that provide a specified accuracy (*e.g.,* accuracy equal to 100%) for both the considered reference observation data-sets $\bar{\mathbf{S}}_\ell(F_1, \mathbf{H}_m)$, $\bar{\mathbf{S}}_\ell(F_0, \mathbf{H}_m)$ as

$$\mathcal{L}_{\mathbf{H}_m} \triangleq \{\ell \in \mathcal{L} : \mathbf{1}_{\mathrm{FR}_\ell > \tau_\ell} \times \mathbf{1}_{\mathrm{NR}_\ell > \tau_\ell} = 1\} \quad (17)$$

with $\mathbf{1}_{x>y}(x)$ being the indicator function for link ℓ: $\mathbf{1}_{x>y}(x) = 1$ if $x > y$ and $\mathbf{1}_{x>y}(x) = 0$ otherwise. The optimal threshold value τ_ℓ for each link is obtained from reference measurements (*i.e.,* non-fall and fall in different directions) during the calibration phase and corresponds to the value of threshold that gives detection accuracy equal or better than a specified value (*e.g.,* usually the target accuracy is set to 100%). In practice, as illustrated in Sect. VI, an interval of threshold values that maximizes the detection accuracy is obtained for each link. The optimal value τ_ℓ is then selected as the mean point of each interval. Finally, these τ_ℓ values are exploited for fall detection in real-time.

Fall detection. For detection of body fall at position $\mathbf{H}_m$, an hard decision metric on each link is adopted:

$$\mathrm{LLR}_\ell(\mathbf{S}_\ell) = \Lambda_\ell\left[\mathbf{S}_\ell|F_1, \mathbf{H}_m\right] - \Lambda_\ell[\mathbf{S}_\ell|F_0, \mathbf{H}_m] \geq \tau_\ell, \quad (18)$$

where LLR and $\mathbf{S}_\ell$ are the log-likelihood ratio and the input RSSI sequence corresponding to an unknown human activity, respectively. A fall event can be detected if the majority of the links votes for the fall event as shown in the decision variable

$$\sum_{\ell\in\mathcal{L}_{\mathbf{H}_m}} \mathbf{1}_{\mathrm{LLR}_\ell(\mathbf{S}_\ell)\geq\tau_\ell} > \sum_{\ell\in\mathcal{L}_{\mathbf{H}_m}} \mathbf{1}_{\mathrm{LLR}_\ell(\mathbf{S}_\ell)<\tau_\ell}. \quad (19)$$

Alternatively, an hard decision metric based only on the likelihood function $\Lambda_\ell\left[\mathbf{S}_\ell|F_1, \mathbf{H}_m\right]$ can be applied as described in [31]. Algorithm 2 describes the DF-FD algorithm focusing on calibration and real time detection for a target located at position $\mathbf{H}_m$.

In the following section, a case study focusing on body fall recognition is described in detail, while detection performance are corroborated by extensive experimental measurements.

Algorithm 2 DF-FD

procedure CALIBRATION ($\mathbf{H}_m$)
  for $\ell = 1 : L$ **do**
    $\{\Delta\mu_\ell(\mathbf{H}_m), \Delta\sigma_\ell(\mathbf{H}_m)\}$ ← build up the RSS map from the reference measurements $\bar{\mathbf{S}}_\ell$ for a target at position $\mathbf{H}_m$
    $\lambda_\ell(F_n|\mathbf{H}_m)$ ← obtain HMM parameters from the map
    τ_ℓ ← obtain optimized threshold using HMM parameters
  end for
  $\mathcal{L}_{\mathbf{H}_m}$ ←link subset selection for real time detection using τ_ℓ (17)
end procedure
procedure REAL TIME DETECTION ($\mathbf{H}_m$)
  for $\ell = 1 : L$ **do**
    $\mathrm{LLR}_\ell(\mathbf{S}_\ell)$ ← compute for each link (18)
  end for
  if $(\sum_\ell \mathbf{1}_{\mathrm{LLR}_\ell(\mathbf{S}_\ell)\geq\tau_\ell} > \sum_\ell \mathbf{1}_{\mathrm{LLR}_\ell(\mathbf{S}_\ell)<\tau_\ell})$ **then**
    Fall detected (19)
  else
    Non-fall
  end if
end procedure

VI. Case study for fall detection (DF-FD)

In this section, a case study focusing on body fall recognition is validated by extensive experimental measurements with artificial and real human subjects, different body structure, age and gender described in the following section. Also, fall event happens at different directions, *i.e.,* backward, forward, lateral left and right, and non-fall measurements obtained when an operator sits on the chair or stands and loses his balance.

Two network configurations are considered: first, detection over a single wireless link is evaluated using software defined radio (SDR) devices implementing an Orthogonal Frequency Division multiplexing (OFDM) transceiver (typically adopted in WiFi physical-layer interfaces), second the joint detection and localization problem is tackled by leveraging an IEEE 802.15.4 standard compliant industrial network implementation. Fall detection performance is evaluated in terms of sensitivity, specificity and accuracy.

A. Network configurations

The network configurations adopted for fall detection performance evaluation are described in the following paragraphs. We implemented two scenarios with one artificial and two real human subjects. In the first scenario, experiments are conducted using a cylindrical anisotropic object, whose surface is covered with adhesive aluminum foils, that mimics a person located in a given position and that falls towards different directions. In order to evaluate the proposed method in a real situation, in the second scenario, the proposed experiments are conducted with two real human subjects with different body structures detailed in Table I. Fall measurements are collected in terms of different pre-impact postures, corresponding to a person that sits on a chair and then falls or stands in a given position and then loses his balance and falls down. The operator maintains the pre-impact posture for 4 seconds and then falls in different directions (fall gesture is repeated 10 times for each direction). RF measurements are also affected by WiFi interference originated by other pre-existing networks deployed in the surrounding area.

Single link configuration. Two SDR devices are deployed in pre-defined positions while exchanging data over 2.4 GHz bands using a IEEE 802.11g-compliant OFDM physical-layer radio interface [32]. As depicted in Fig. 4, a single antenna transmitter (TX) is communicating with a receiver (RX). The received data is then sent to the processing unit that monitors the RSSI samples along the path between the TX and RX. The physical layer signal strength (*i.e.,* RSSI) relates to one OFDM pilot sub-carrier. The RSSI samples are recorded every $\Delta t = 20\ \mu s$ over consecutive OFDM symbols of duration 16 μs each. Each RSSI sequence (or footprint) has a duration of 10 seconds.

Distributed network configuration. The second network configuration, used for experimental validation, is based on a deployment of $N = 12$ IEEE 802.15.4 devices communicating over a full mesh topology. Each RF device features a NXP JN5148 single-chip micro-controller based on IEEE802.15.4 standard for RF node. The RSSI dynamic range for each RF node is 75dB with a minimum sensitivity of about -95dBm. For all tests, we employed omni-directional, vertically polarized antennas, with a gain of 2dBi. The RF nodes are configured to transmit with the output power set to 0 dBm [21].

The network includes 11 field devices, one network coordinator (NC) device (see Fig. 5) and a processing unit (that might be physically separated from the NC). Wireless nodes (*i.e.,* all nodes except the NC) synchronize to the beacon-frames transmitted by the NC node itself. The proposed MAC sublayer uses a timed-token message passing protocol redesigned on top of the beacon-enabled mode of the IEEE 802.15.4 standard to periodically synchronize the network.

Each device is configured to wait for the token message: in case of a packet drop, a real-time error controller guarantees the generation of a new token after the time-to-token-visit listening time expires. Details about the time-slotted protocol are given in reference [21]; moreover, they perform a periodic and synchronous transmission of IEEE 802.15.4 frames over reserved time-slots, measure the RSSI values from the received signals and forward the RSSI data to the NC device.

As discussed in Sect. IV, during real-time fall detection, RSSI measurements are recorded every $\Delta t = 60\ ms$ while location estimates are refreshed every T_R = 360 ms. The sampling interval for RSSI data is set to allow a real-time acquisition of $L/\Delta t = 2200$ links/s where $L = N(N-1) = 132$. This sampling interval is kept small enough to capture all the human activity profiles of interest. Body fall detection is refreshed every T_R.

The system can monitor the operator inside the detection zone with walls and obstacles and active/pre-existing WiFi interference. Wireless modules operate in the 2.4 GHz band and

TABLE I
FALL SCENARIO PROFILE

Subject	Height	Weight/Diameter	Age	Gender
1	1.60 m	60 kg / –	34	male
2	1.81 m	95 kg / –	58	male
3	1.80 m	1 kg / 30 cm	–	artificial object

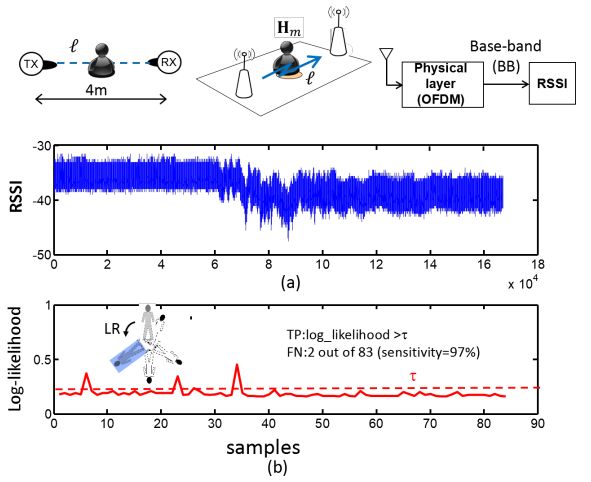

Fig. 4. (a) RSSI footprints and (b) Fall detection log-likelihood using the software defined radio-SDR configuration in real-time.

collect all RSSI measurements in real-time (over bi-directional wireless links). Being an experimental setup, during network start-up only a standard interference avoidance mechanism is applied so that the best IEEE 802.15.4 channel [33] is automatically selected to avoid co-channel interference (*i.e.,* from WiFi/Bluetooth devices). More complex interference avoidance schemes can be adopted but they are outside the scope of this paper.

B. Performance evaluation

Fall detection experiments have been carried out using both network configurations mentioned in Sect. VI-A, with a target placed at the same position $\mathbf{H}_m$ but falling in different directions *i.e.,* forward, backward, lateral left and lateral right.

In the SDR configuration, fall detection is implemented using measurements obtained from a single-link configuration while performance is evaluated in terms of sensitivity as defined in Table II. In Fig. 4 (b), we recall here that a simple hard decision on observed likelihoods [31] is sufficient to obtain 97% of fall detection sensitivity. However, the above tests are limited to a single link, and useful only for the purpose of fall detection of a fixed target in a given location and according to a specific fall direction.

The distributed network configuration is a more useful setup for the large number of links that can be selected for detection (in our case, $L = 132$ links) even if this increases the processing capability requirements.

Fig. 6 shows the fall detection results by computing the log-likelihood ratio LLR for a single link, *i.e.,* connecting device 5 and 10, corresponding to falls in the forward, backward, lateral

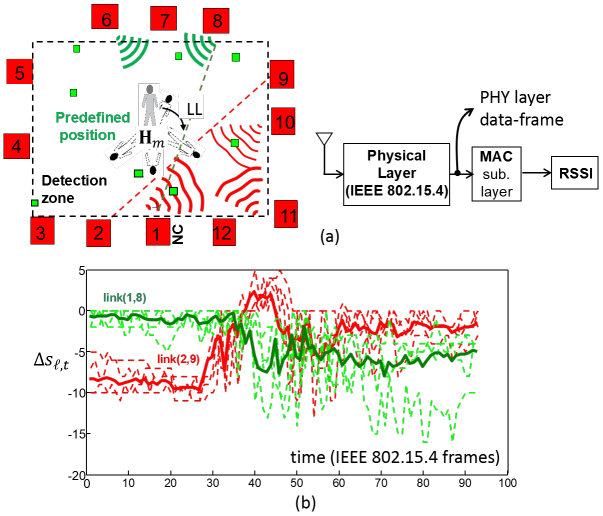

Fig. 5. (a) Network configuration, (b) RSSI perturbations (dashed lines) for two selected links, with superimposed average footprints (solid lines).

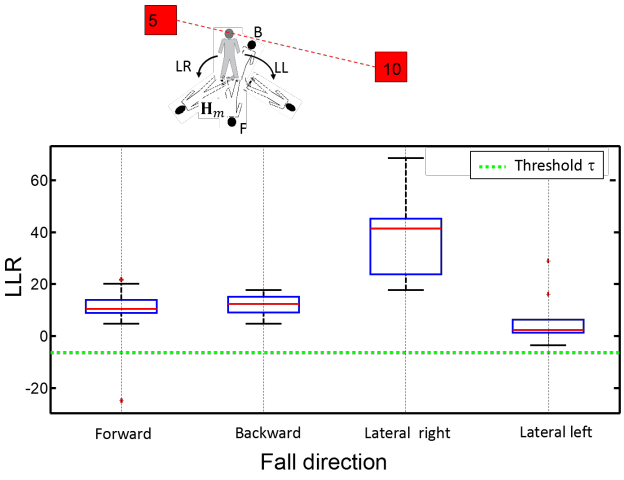

Fig. 6. Log-likelihood ratio-LLR and fall detection for a single link (link 5-10) at four different directions (*i.e.,* forward, backward, lateral left, and lateral right).

left and lateral right directions. As shown in this figure, the single-link detector is not accurate enough, since some errors are observed for detection of fall in the forward direction.

In order to reduce the algorithm complexity but improve the detection performances with respect to the single-link case, optimal link selection is therefore carried out during the calibration of the multi-link configuration. During this phase, two reference data sets corresponding to fall state measurements $\overline{\mathbf{S}}_\ell = \overline{\mathbf{S}}_\ell(F_1, \mathbf{H}_m)$ and non-fall ones $\overline{\mathbf{S}}_\ell = \overline{\mathbf{S}}_\ell(F_0, \mathbf{H}_m)$ have been employed to train all single-link detectors and to obtain the performance metrics for all detectors.

The collected RSSI measurements provide a representative data-set for body fall towards all the pre-defined directions, as well as for body in safe-state (non-fall measurements corresponding to a person maintaining a safe posture, without falling). The optimized link set $\mathcal{L}_{\mathbf{H}_m}$ and the optimized threshold τ_ℓ are evaluated by selecting only the links that provide the highest accuracy figures. Fig. 7 shows the selected

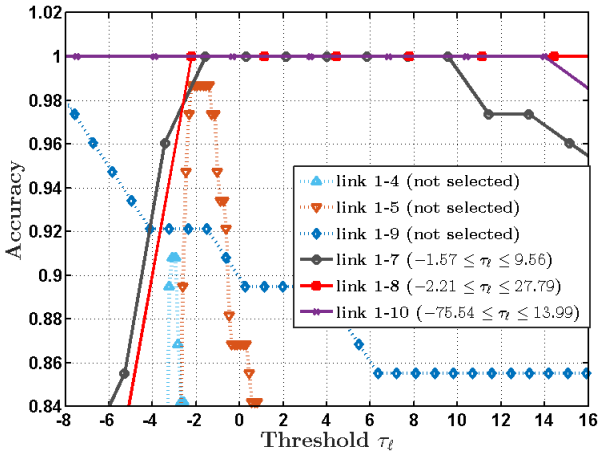

Fig. 7. Link subset selection and threshold τ_ℓ optimization: optimal links 1-7, 1-8 and 1-10 are selected (*i.e.,* for each link, there is an interval of threshold values that gives accuracy = 100%) while sub-optimal ones 1-4, 1-5 and 1-9 are discarded.

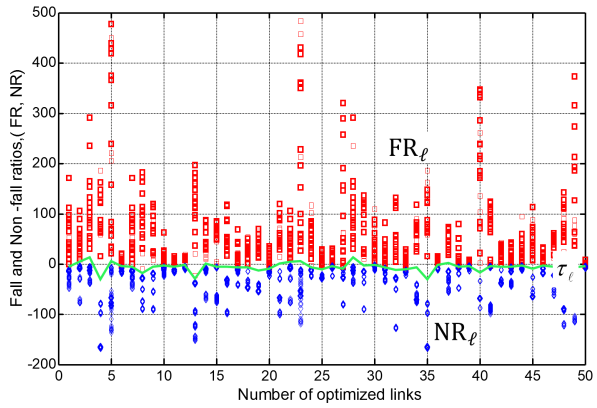

Fig. 8. Fall (red squares) and non-fall (blue squares) ratios (*i.e.,* FR and NR) for the selected links and corresponding optimized thresholds in solid line.

links 1-7, 1-8, 1-10 from Fig. 5 (a) and the corresponding threshold intervals that maximize the accuracy with respect to the training RSSI measurements (recall that the optimal threshold value τ_ℓ corresponds to the mean point of each interval). Herein, only 50 out of 132 links have been selected by the aforementioned procedure.

Decision about the fall/non-fall detection event is based on major voting (19) over the optimized link subset. Fig. 8 shows the log-likelihood ratio corresponding to fall (15) and non-fall (16) reference measurements for the optimized link subset, compared against the optimized threshold τ_ℓ.

After link optimization, validation of the detection results is based on a second data-set of fall and non-fall RSSI measurements having the same size of the training one. For performance assessment, the following metrics have been computed for each link: sensitivity, specificity, accuracy, false positive rate and F-1 score. Their definition is recalled in Table II. These metrics refers to the TP (True Positive), TN (True Negative), FP (False Positive) and FN (False Negative) quantities computed for each trained detector during the verification

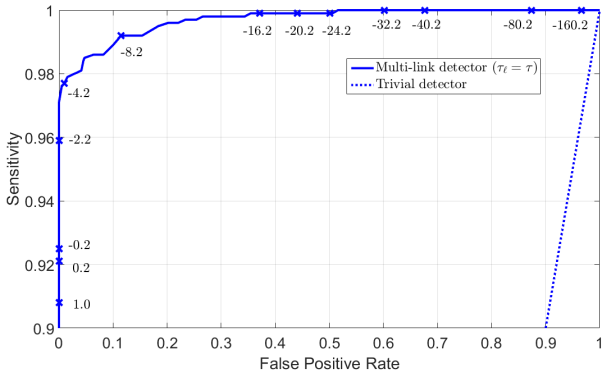

Fig. 9. Receiver operating characteristic (ROC) curve for multi-link fall detection over the optimized links. Some threshold values τ are superimposed over the ROC curve.

TABLE II
STATISTICAL PERFORMANCE METRICS FOR FALL DETECTION

Sensitivity (TPR)	$\frac{TP}{TP+FN}$	TP:true positive FN:false negative
Specificity	$\frac{TN}{TN+FP}$	TN:true negative FP:false positive
Accuracy	$\frac{TP+TN}{N+P}$	N:number of non-fall measurements P:number of fall measurements
F-1 score	$\frac{2TP}{2TP+FP+FN}$	-
False positive rate-FPR	$\frac{FP}{N}$	-

TABLE III
FALL DETECTION PERFORMANCES USING 50 OPTIMIZED LINKS OVER 4488 TESTS IN DIFFERENT DIRECTIONS

Sensitivity	Specificity	Accuracy	F-1	FPR
0.97	0.99	0.98	0.98	0.007

phase.

Table III summarizes the fall/non-fall detection capabilities in terms of detector metrics (*i.e.,* sensitivity, specificity, accuracy, false positive rate, and F-1 score) using the optimized thresholds of the link subset. These results confirm the good performances of the proposed fall detection system for different falling directions and extend the single-link ones [31] obtained only for a given direction.

The ROC curve of the complete fall detection system, including the non-fall and fall measurements in four directions, is depicted in Fig. 9. The curve is obtained by comparing the sensitivity versus the false positive rate, after multi-link selection (*i.e.,* 50 links) and according to the majority voting scheme (19). To plot this curve, a single threshold value τ is now used for all link detectors: $\forall \ell = 1,..,50\ \tau_\ell = \tau$. The ROC curve is also based on the same selected subset of links, chosen during multi-link calibration. Sensitivity corresponds to the fall event measurements (towards all the pre-defined directions) and it is computed using Table II for each link by comparing the fall likelihood ratio in (15) with respect to the corresponding threshold value τ_ℓ for a given link ℓ. False Positive ratio is obtained from non-fall measurements

by comparing the non-fall likelihood ratio in (16) with respect to the corresponding threshold value τ_ℓ for a given link. The performances of the random detector (known also as the trivial detector) are also shown for comparison.

VII. Conclusion

The paper describes a RF-based network system that processes the received signal strength information for the joint purpose of human localization and detection of body falling. The proposed detection algorithm is based on Hidden Markov Model techniques and exploits RF signal perturbations (sensorless), obtained from a distributed network of wireless devices deployed around a workspace. The proposed system can be used to extract information about human location, motion and health-critical posture features. According to the specific application of fall detection, the system is devised to enrich the range of sensors, which currently are the key-point of workers safety and protection in industrial applications. Moreover, the system provides also a source of target information to be possibly fused with other sensor sources *e.g.,* environmental cameras, if available. Experimental activity has been conducted to validate both target localization and fall detection algorithms and evaluate their performances. Preliminary results confirm the effectiveness of the proposed approach in terms of sensitivity and specificity to detect fall events.

References

[1] R. Igual, C. Medrano, and I. Plaza, "Challenges, issues and trends in fall detection systems," *Journal Biomed. Eng. Online*, vol. 12, no. 66, pp. 1-66, Jul. 2013.

[2] L.D Xu, W. He, and S. Li, "Internet of Things in industries: A survey," *IEEE Trans on Industrial Informatics*, vol. 10, no. 4, pp. 2233-2243, Nov. 2014.

[3] A. Yachir, Y. Amirat, A. Chibani, and N. Badache, "Event-aware framework for dynamic services discovery and selection in the context of ambient intelligence and internet of things," *IEEE Trans. on Automation Science and Engineering*, vol. 13, no. 1, pp. 85-102, Jan. 2016.

[4] S. Savazzi, S. Sigg, M. Nicoli, V. Rampa, S. Kianoush, and U. Spagnolini, "Device-free radio vision for assisted living: leveraging wireless channel quality information for human sensing," *IEEE Signal Processing Magazine*, vol. 33, no. 2, pp. 45-58, Mar. 2016.

[5] H.M Ashfak, Mas S. Mohktar, S. B. Kamaruzzaman, K.S Lim, T.M Pin, and F. Ibrahim, "Smartphone-based solutions for fall detection and prevention: challenges and open issues," *Sensors Journal*, vol. 14, no. 4, pp. 7181-7208, Apr. 2014.

[6] H. Rimminen, J. Lindstrom, M. Linnavuo, and R. Sepponen, "Detection of falls among the elderly by a floor sensor using the electric near field," *IEEE Trans. on Inf. Technol. in Biomed.*, vol. 14, no. 6, pp. 1475-1476, Nov. 2010.

[7] C.L Wu, Y.S Tseng, and L.C Fu, "Spatio-temporal Feature Enhanced Semi-supervised Adaptation for Activity Recognition in IoT-Based Context-Aware Smart Homes," *Proc. of IEEE International Conference on Internet of Things*, pp. 460-467, Aug. 2013.

[8] L. Hui, H. Darabi, P. Banerjee, and J. Liu, "Survey of wireless indoor positioning techniques and systems," *IEEE Trans. on Systems, Man, and Cybernetics, Part C (Applications and Reviews),* vol. 37, no. 6, pp. 1067-1080, Nov. 2007.

[9] S. Kim, C. Mariotti, F. Alimenti, P. Mezzanotte, A. Georgiadis, A. Collado, L. Roselli, and MM. Tentzeris, "No battery required: perpetual RFID-enabled wireless sensors for cognitive intelligence applications," *IEEE Microwave Magazine*, vol. 14, no. 5, pp. 66-77, Jul. 2013.

[10] M. Yuwono, B. Moulton, S. Su, B. Celler, and H. Nguyen, "Unsupervised machine-learning method for improving the performance of ambulatory fall-detection systems," *Journal Biomed. Eng. Online* , pp. 1-11, Feb. 2012.

[11] J. Cheng, C. Xiang, and S. Minfen, "A framework for daily activity monitoring and fall detection based on surface electromyography and accelerometer signals," *IEEE Journal Biomed. and Health Inform.*, vol. 17, no. 1, pp. 38-45, Jan. 2013.

[12] N. Patwari, N. Ash Joshua, and N.S. Correal, "Locating the nodes: cooperative localization in wireless sensor networks," *IEEE Signal Processing Magazine*, vol. 22, no. 4, pp. 54-69, Jul. 2005.

[13] M.A. Labrador, and O.D. Lara Yejas, "Human activity recognition: Using wearable sensors and smartphones," *Chapman and Hall/CRC*, 2013.

[14] T. Teixeira, G. Dublon, A. Savvides, "A survey of human-sensing: Methods for detecting presence, count, location, track, and identity, "ACM Computing Surveys, no. 5, pp. 427-450, Sep. 2010.

[15] S. Sigg, M. Scholz, S. Shi, Y. Ji, and M. Beigl, "RF-sensing of activities from non-cooperative subjects in device-free recognition systems using ambient and local signals," *IEEE Trans. on Mobile Computing*, vol. 13, no. 4, pp. 907-920, Apr. 2014.

[16] C. Liu, C. Lee, and P. Lin, "A fall detection system using k-nearest neighbor classifier," *IEEE Journal on Real-Time Image Processing*, vol. 37, no. 10, pp. 7174-7181, Oct. 2010.

[17] Y. Li, KC. Ho, and M. Popescu, "A microphone array system for automatic fall detection," *IEEE Trans. on Biomed. Eng.*, vol. 59, no. 5, pp. 1291-1301, May 2012.

[18] C. Rougier, J. Meunier, A. St-Arnaud, and J. Rousseau, "Robust video surveillance for fall detection based on human shape deformation," *IEEE Trans. on Circuits and Systems for Video Technology*, vol. 21, no. 5, pp. 611-622, May 2011.

[19] A. Saeed, A.E. Kosba, and M. Youssef, "Ichnaea: A low-overhead robust WLAN device-free passive localization system," *IEEE Journal on Sel. Topics in Signal Processing*, vol. 8, no.1, pp. 5-15, Feb. 2014.

[20] J. Wilson, and N. Patwari, "Radio tomographic imaging with wireless networks," *IEEE Trans. on Mobile Computing*, vol. 9, no. 5, pp. 621-632, May 2010.

[21] S. Savazzi, V. Rampa, F. Vicentini, and M. Giussani, "Device-free human sensing and localization in collaborative human-robot workspaces: a case study," *IEEE Sensors Journal*, vol. 16, no. 5, pp. 1253-1264, Mar. 2016.

[22] V. Rampa. S. Savazzi, M. Nicoli, and M. D' Amico, "Physical Modeling and performance bounds for Device-Free Localization Systems," *IEEE Signal processing letters*, vol. 22, no. 11, pp. 1864-1868, Nov. 2015.

[23] M. Scholz, L. Kohout, M. Horne, M. Budde, M. Beigl, and M. A. Youssef, "Device-free radio-based low overhead identification of subject classes," *Proc. of the 2nd Workshop on Physical Analytics (WPA'15),* pp. 1-6, May 2015.

[24] F. Sergi, G. Alenya, and C. Torras, "Lock-in time-of-flight (ToF) cameras: a survey," *IEEE Sensors Journal*, vol. 11, no. 9, pp. 1917-1926, Sep. 2011.

[25] *IEEE Standard for a precision clock synchronization protocol for networked measurement and control systems*, IEC 61588:2009(E), 2009,

[26] S. Kianoush, V. Rampa, S. Savazzi, and M. Nicoli, "Pre-deployment performance assessment of device-free radio localization systems," *Proc. of the IEEE Intl. Conf. on Commun. (ICC'2016)*, Kuala Lumpur, May 2016.

[27] A. G. O. Mutambara, "Information based estimation for both linear and nonlinear systems," *Proc. of the 1999 American Control Conference*, vol. 2, pp. 1329-1333, Jun. 1999.

[28] J.Z. Sasiadek, and P. Hartana, "Sensor data fusion using Kalman filter," *Proc. of the Third International Conference on Information Fusion (FUSION 2000)*, vol. 2, pp. WED5/19 - WED5/25, Jul. 2000.

[29] G. H. Weiss and R. J. Rubin, "Random Walks: Theory and selected applications," *Adv. in Chem. Phys.*, vol. 52, pp. 363-505, Jan. 1982.

[30] L. Rabiner, "A tutorial on Hidden Markov Models and selected applications in speech recognition," *Proc. of the IEEE,* vol. 77, no. 2, pp. 257-286, Feb. 1989.

[31] S. Kianoush, S. Savazzi, F. Vicentini V. Rampa, and M. Giussani, "Leveraging RF signals for human sensing: fall detection and localization in human-machine shared workspaces," *13th IEEE International Conference on Industrial Informatics (INDIN'15),* pp. 1456-1462, Jul. 2015.

[32] B. Bloessl, M. Segata, C. Sommer, and F. Dressler, "An IEEE 802.11a/g/p OFDM Receiver for GNU Radio," *2nd ACM SIGCOMM Workshop of Software Radio Implementation Forum (SRIF'13),* pp. 9-16, Aug. 2013.

[33] *IEEE Standard for Local and metropolitan area networks*, Part 15.4: Low-Rate Wireless Personal Area Networks (LR-WPANs) Amendment 1: MAC sublayer, 802.15.4e, 2012.